East European Journal of Physics. 4. 575-581 (2025)
DOI:10.26565/2312-4334-2025-4-60 ISSN 2312-4334

DEVELOPMENT AND EVALUATION OF 3D-PRINTED HOMOGENEOUS AND HETEROGENEOUS PHANTOMS FOR QUALITY ASSURANCE IN RADIATION THERAPY

V. Vashchyshyn[1]*, O. Bezshyyko[2§], L. Golinka-Bezshyyko[2]
[1]Radiotherapy Department, Universal Clinic "Oberig", Kyiv, Ukraine
[2]Taras Shevchenko National University of Kyiv, Kyiv, Ukraine
**Corresponding Author E-mail: v.vashchyshyn@oberig.ua; [§]obezsh@gmail.com*
Received August 2, 2025; revised September 15, 2025; accepted September 30, 2025

Background: Affordable and locally manufacturable quality assurance (QA) phantoms are critical for maintaining accuracy in radiation therapy, particularly in low-resource settings. This study evaluates the radiological and dosimetric performance of 3D-printed homogeneous and heterogeneous phantoms against commercial standards.

Methods: Two phantom prototypes were developed: a homogeneous model fabricated from PMMA and a heterogeneous model composed of EVA, PLA, MDI-based foam, and gypsum–chalk composite. Radiological properties were assessed using CT imaging with three reconstruction kernels (Hp38, Bf39, Hr32) at slice thicknesses of 1–3 mm. Hounsfield Units (HU) were compared with reference values from the Easy Slab (IBA) and CatPhan 604. Dosimetric validation was performed with Eclipse TPS (v16.1) using 15 3D-CRT and 15 VMAT plans, delivered on Varian TrueBeam (6 MV, 6 MV FFF, 10 MV, 10 MV FFF) and Halcyon (6 MV FFF) accelerators. Point doses were measured with a calibrated Farmer chamber.

Results: The homogeneous PMMA phantom demonstrated HU stability within ±5 HU of the reference values across all kernels, with standard deviations of less than 3 HU. EVA and gypsum–chalk provided tissue-equivalent and bone-equivalent imaging properties (20 ± 3 HU and 1200 ± 15 HU, respectively), while PLA and MDI foam demonstrated excessive variability (>40 HU kernel dependence). Dosimetrically, the homogeneous phantom achieved agreement with TPS calculations within ±2.5% across all energies and techniques. The heterogeneous phantom exhibited deviations of up to 2.8%, remaining within the ±3% tolerance of AAPM TG-119. Variability was most significant for VMAT plans with FFF beams, particularly on the Halcyon platform.

Conclusion: A 3D-printed homogeneous PMMA phantom demonstrated radiological stability and dosimetric accuracy comparable to that of commercial devices, confirming its feasibility for routine QA. The heterogeneous model exhibited acceptable performance but requires material refinement, particularly substitution of PLA and MDI foam, to improve HU stability. These results highlight the potential of additive manufacturing to provide cost-effective, customizable QA solutions for radiation therapy, especially in resource-limited environments.

Keywords: *Quality assurance (QA); 3D printing in medical physics; Imaging phantoms; Computed tomography (CT); HU stability; End-to-end testing; Phantom validation; Affordable QA devices*
PACS: 7.57.Q–

1. INTRODUCTION

Quality assurance (QA) in radiation therapy is critical to ensure accurate dose delivery and patient safety, in line with international recommendations [1]. QA phantoms play a central role in these procedures, providing reproducible conditions for imaging, treatment planning, and end-to-end verification.

In recent years, additive manufacturing (3D printing) has emerged as a promising approach for producing custom QA devices. A growing body of literature has demonstrated the feasibility of 3D-printed phantoms for imaging and dosimetry [2]. For example, Kunert et al. developed realistic 3D-printed body phantoms and compared measured and simulated organ doses in CT of a pregnant woman [3]. Other studies have investigated the impact of material composition and characterized the mechanical and imaging properties of commonly used 3D-printed plastics [4, 5]. Zain et al. reported dosimetric characterization of customized PLA phantoms, showing agreement with solid water within clinically acceptable limits [6].

Systematic reviews confirm that most prior works have focused on thoracic or homogeneous slab models [7]. By contrast, heterogeneous anthropomorphic designs have been evaluated for lung [8], head-and-neck [9, 10], and brain stereotactic radiosurgery applications [11]. Moreover, comprehensive end-to-end tests combining dosimetric and geometric verification have also been reported [12], though such studies remain relatively few.

Despite these advances, the majority of 3D-printed phantoms remain limited in their ability to reproduce heterogeneous tissue properties or to undergo full clinical validation with advanced delivery techniques such as VMAT. This gap is particularly relevant for low- and middle-income countries, including Ukraine, where resource constraints frequently restrict access to advanced QA infrastructure and cost-effective alternatives are urgently needed [13].

2. MATERIALS AND METHODS

2.1. Phantom Design and Fabrication

Two phantom prototypes were designed and fabricated using fused deposition modeling (FDM) 3D printing technology:

Cite as: V. Vashchyshyn, O. Bezshyiko, L. Golinka-Bezshyyko, East Eur. J. Phys. 4, 575 (2025), https://doi.org/10.26565/2312-4334-2025-4-60

1. **Homogeneous phantom** — manufactured entirely from polymethyl methacrylate (PMMA) to provide a uniform electron density.
2. **Heterogeneous phantom** — composed of multiple materials to simulate soft tissue and bone:

- EVA (ethylene-vinyl acetate) — soft tissue surrogate.
- PLA (polylactic acid) — dense soft tissue surrogate.
- MDI-based rigid polyurethane foam — low-density lung-equivalent material.
- Gypsum–chalk composite — cortical bone surrogate.

Design schematics were created in *Autodesk Fusion 360* and exported as STL files for printing. The phantoms were printed using an *Ultimaker S5* 3D printer with 0.4 mm nozzle, 0.2 mm layer height, and 100% infill for PMMA and PLA components. EVA and MDI foams were cut to shape and inserted into designated cavities. The overall dimensions of each phantom matched those of the commercial Easy Slab phantom, allowing for direct performance comparison.

2.2. Reference Phantoms

For benchmarking, two commercially available phantoms were used (Fig. 1):

- **Easy Slab** (IBA Dosimetry, Germany) — a homogeneous PMMA phantom for reference dosimetry and QA.
- **CatPhan 604** (The Phantom Laboratory, USA) — a diagnostic imaging QA phantom.

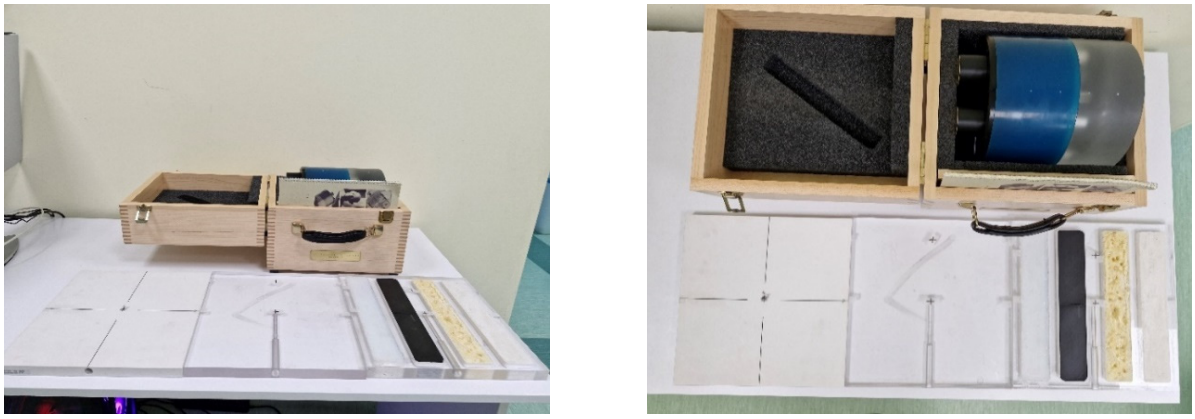

Figure 1. Photograph of the homogeneous and heterogeneous 3D-printed phantoms alongside the IBA Easy Slab and CatPhan 604.

2.3. Radiological Evaluation

2.3.1. CT Acquisition

Radiological properties of all materials were evaluated using a *Siemens SOMATOM Confidence* large-bore CT scanner. Scans were performed at 120 kVp, 250 mAs, with 500 mm field of view (FOV). Slice thicknesses of **1 mm** and **3 mm** were acquired with three reconstruction kernels:

- Hp38 — standard head protocol
- Bf39 — body filter
- Hr32 — high-resolution protocol

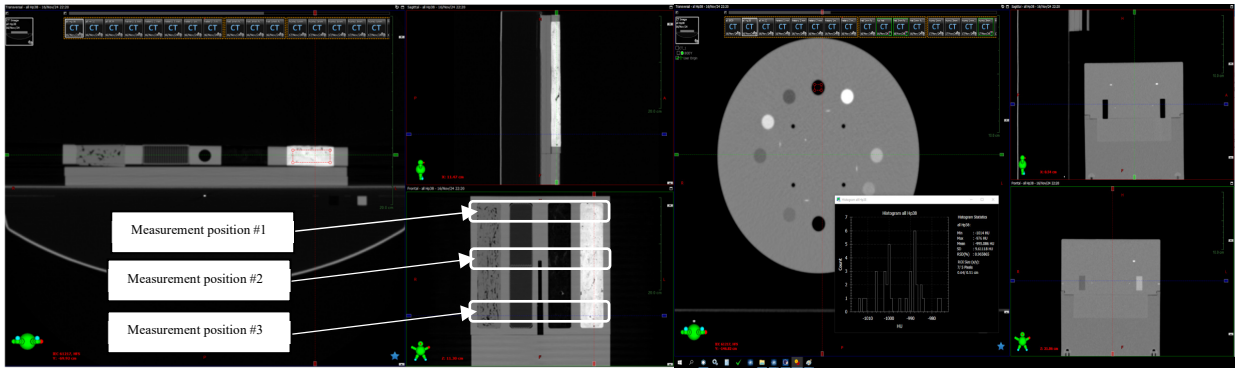

Figure 2. Axial CT slices of phantoms scanned with Hr32 kernel

For each material insert, rectangular regions of interest (ROIs) of 1 cm² were placed in proximal, central, and distal slices using *Eclipse Varian* software (Figure 2). Mean Hounsfield Units (HU) and standard deviations (SD) were recorded.

2.4. Dosimetric Validation

2.4.1. Treatment Planning

End-to-end dosimetric testing was performed using the Eclipse v16.1 treatment planning system (Varian Medical Systems, USA) with AcurosXB dose calculation algorithm on the ARIA oncology platform. For each phantom, 15 three-dimensional conformal radiotherapy (3D-CRT) plans and 15 volumetric modulated arc therapy (VMAT) plans were created. Plans were calculated for the following beam energies:

- Varian TrueBeam 2.7: 6 MV, 6 MV FFF, 10 MV, 10 MV FFF
- Varian Halcyon: 6 MV FFF only

All plans prescribed a dose to isocenter, normalized to 100% at the ion chamber location.

2.4.2 Measurement Setup

Point dose measurements were performed using a calibrated Farmer-type ionization chamber (FC65P, IBA) connected to a DOSE1 electrometer. The chamber was placed in a central cavity of each phantom with a 5 cm water-equivalent buildup upstream (Fig. 3). Temperature and pressure corrections were applied according to IAEA TRS-398 formalism [12].

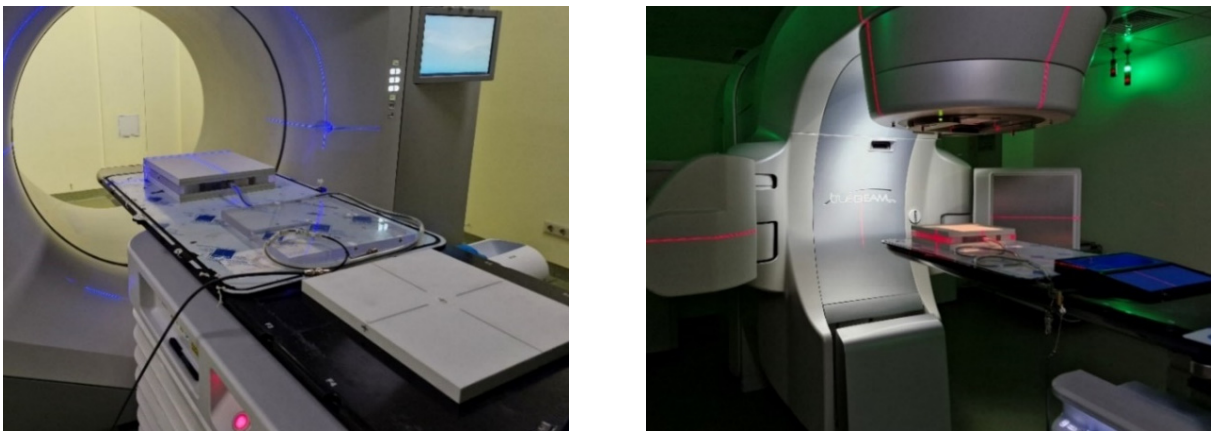

Figure 3. Photograph of measurement setup on TrueBeam with phantom and ionization chamber in position.

2.5 Data Analysis

Measured doses were compared with TPS-calculated doses, and percentage differences were computed:

$$\Delta D(\%) = \frac{D_{meas} - D_{TPS}}{D_{TPS}} \times 100$$

Acceptance criteria followed AAPM TG-119 recommendations, with ±3% considered clinically acceptable [2]. HU variations > 40 HU were considered significant.

3. Results

3.1 Radiological evaluation

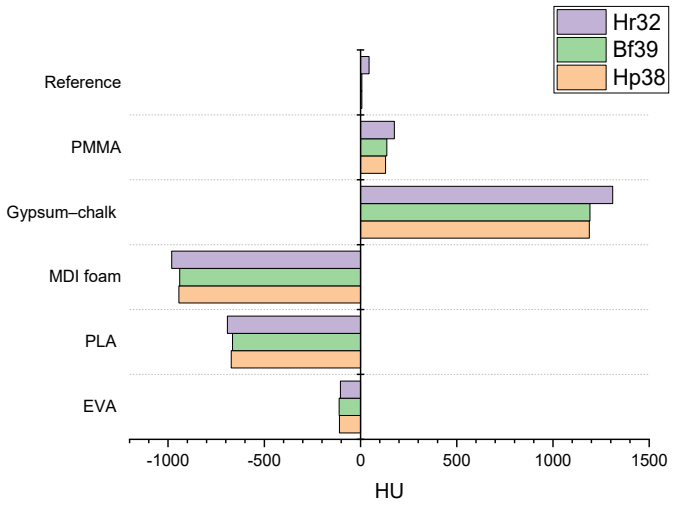

Figure 4. Materials HU variations across different kernels

The homogeneous PMMA phantom demonstrated highly consistent HU values across all three reconstruction kernels, with variations remaining within ±5 HU across different slice positions and acquisition protocols. EVA and the gypsum–chalk composite in the heterogeneous phantom showed stable and reproducible values that align with the expected ranges for soft tissue–like and bone-like surrogates, respectively. In contrast, PLA and MDI-based foam exhibited greater variability, particularly when reconstructed with the Hr32 kernel, where fluctuations exceeded ±40 HU (Figure 4).

Despite these differences, the overall stability of PMMA, EVA, and gypsum–chalk ensured cohesive and clinically interpretable results in subsequent end-to-end testing.

Table 1 summarizes the mean HU values and standard deviations for all materials and kernels, based on measurements in proximal, central, and distal slices.

Table 1. HU mean ± SD for all materials and kernels (Hp38, Bf39 and Hr32)

Hp38	Min HU	Max HU	Mean HU	Average SD, HU	SD/mean in %
air	-1014	-976	-995.1	**9.6**	0.97
PMP	-194	-137	-177.5	**14.6**	8.2
Bone 50%	582	634	608	**12.8**	2.1
LDPE	-111	-55	-84.8	**13.7**	16.1
Polystyrene	-54	-17	-34.6	**9**	26
Acrylic	106	142	125.3	**9.2**	7.4
Bone 20%	167	232	201.4	**16.7**	8.3
Delrin	332	376	350.6	**11.6**	3.3
Teflon	891	957	921.4	**17**	1.8
Heterogeneous 1	-792.3	-13.3	-109.0	**134.1**	124.7
Heterogeneous 2	-739.7	-601.3	-671.9	**32.8**	4.87
Heterogeneous 3	-1007.3	-709.7	-943.7	**39.8**	4.2
Heterogeneous 4	325.7	1402	1188.2	**124.1**	10.5
Homogeneous	98	161	129.9	**10.8**	8.3
Reference	-18.3	41.7	6.7	**7.8**	159.9
Bf39	Min HU	Max HU	Mean HU	Average SD, HU	SD/mean, %
air	-1024	-953	-982.5	**15.1**	1.5
PMP	-206	-137	-171.7	**16**	9.4
Bone 50%	555	631	593.4	**19.5**	3.3
LDPE	-125	-49	-85.7	**18.3**	21.4
Polystyrene	-67	-2	-35.1	**16.9**	48.1
Acrylic	105	145	123.6	**13.1**	10.6
Bone 20%	163	203	186.4	**9.7**	5.2
Delrin	314	374	336.8	**17.4**	5.2
Teflon	880	937	906.5	**15.3**	1.7
Heterogeneous 1	-782	-14.3	-111.2	**127.9**	115.4
Heterogeneous 2	-777	-558	-665.5	**55.6**	8.3
Heterogeneous 3	-1014.7	-753.3	-940.1	**37.8**	4.1
Heterogeneous 4	684	1485	1192.3	**113.0**	9.4
Homogeneous	82.7	178.7	136.7	**13.8**	10.1
Reference	-26	41.7	7.1	**11.2**	180.7
Hr32	Min HU	Max HU	Mean HU	Average SD, HU	SD/mean in %
air	-1024	-1021	-1022	**0.8**	0.1
PMP	-232	-184	-213	**14.7**	6.9
Bone 50%	674	716	693.6	**11.3**	1.6
LDPE	-117	-93	-103.5	**6.9**	6.7
Polystyrene	-56	-32	-45.1	**6.6**	14.6
Acrylic	123	144	136.2	**5.1**	3.8
Bone 20%	211	245	224.4	**10.4**	4.6
Delrin	383	416	401.1	**9**	2.2
Teflon	1051	1093	1064	**12**	1.1
Heterogeneous 1	-830.3	9	-104.6	**145.4**	141.6
Heterogeneous 2	-746.7	-629.3	-691.6	**29.2**	4.2
Heterogeneous 3	-1024	-752	-981.7	**46.5**	4.8
Heterogeneous 4	731.3	1520.7	1310.2	**98.6**	7.5
Homogeneous	151	207.7	175.6	**10.2**	5.8
Reference	24.3	67.3	44.4	**7.7**	17.1

3.1.2 Slice thickness and kernel effects

Reduction of slice thickness from 3 mm to 1 mm had negligible impact on HU values for PMMA and EVA but slightly increased variability in low-density materials such as MDI foam. Kernel selection had the largest influence on high-density materials (gypsum–chalk) and on the unstable components (PLA, MDI), reinforcing the need for material optimization in heterogeneous designs.

3.2 Dosimetric validation

End-to-end dosimetric testing demonstrated strong agreement between TPS-calculated and measured point doses for both phantoms (Table 2). The homogeneous PMMA phantom achieved excellent consistency, with discrepancies across all energies and delivery techniques remaining within ±2.5%. The heterogeneous phantom also performed within the clinically acceptable ±3% TG-119 threshold, with a maximum deviation of 2.8%.

Table 2. Measured vs. TPS dose comparison for all phantoms and energies

TrueBeam		3D CRT			VMAT		
		Meas mean, Gy	TPS, Gy	%, diff	Meas mean, Gy	TPS, Gy	%, diff
Homo	6MV	2.016	2.040	**1.17**	2.041	2.092	**2.50**
	6FFF	2.025	2.042	**0.82**	2.055	2.101	**2.24**
	10MV	1.999	2.014	**0.75**	2.046	2.084	**1.86**
	10FFF	2.038	2.051	**0.65**	2.046	2.097	**2.49**
Hetero	6MV	2.027	2.038	**0.56**	2.049	2.065	**0.78**
	6FFF	2.063	2.039	**-1.18**	2.050	2.042	**-0.38**
	10MV	2.003	2.018	**0.73**	2.055	2.105	**2.45**
	10FFF	2.050	2.043	**-0.34**	2.090	2.081	**-0.43**
Ref	6MV	2.110	2.041	**-3.25**	2.042	2.043	**0.05**
	6FFF	2.032	2.028	**-0.21**	2.059	2.044	**-0.73**
	10MV	2.001	2.043	**2.12**	2.042	2.080	**1.86**
	10FFF	2.041	2.067	**1.29**	2.065	2.057	**-0.39**

Halcyon	3D CRT			VMAT		
	Meas mean, Gy	TPS, Gy	%, diff	Meas mean, Gy	TPS, Gy	%, diff
Homo	2.062	2.069	-0.34	2.029	2.034	-0.25
Hetero	2.068	2.081	-0.62	2.030	2.041	-0.52
Ref	2.060	2.057	0.15	2.035	2.037	-0.11

A clear trend was observed between accelerators: Halcyon measurements showed smaller discrepancies overall compared to TrueBeam, reflecting the stable modeling of the 6 MV FFF beam in Eclipse. On the TrueBeam, slightly larger variations appeared, particularly in cases involving heterogeneous material inserts, likely due to increased sensitivity to density inhomogeneities and geometric setup factors.

No systematic differences were detected between 3D-CRT and VMAT techniques. Both delivery approaches yielded comparable agreement with TPS predictions, indicating that plan complexity did not substantially influence phantom performance. This finding suggests that the observed deviations are primarily attributable to material properties and beam modeling, rather than delivery method.

Figure 5 illustrates these outcomes, showing tight clustering of measured-to-TPS dose ratios around unity for the homogeneous phantom, and somewhat broader but still clinically acceptable distributions for the heterogeneous phantom. Together, these results confirm the suitability of the homogeneous phantom for clinical QA across diverse energies and delivery techniques, while highlighting opportunities for refinement in the heterogeneous design.

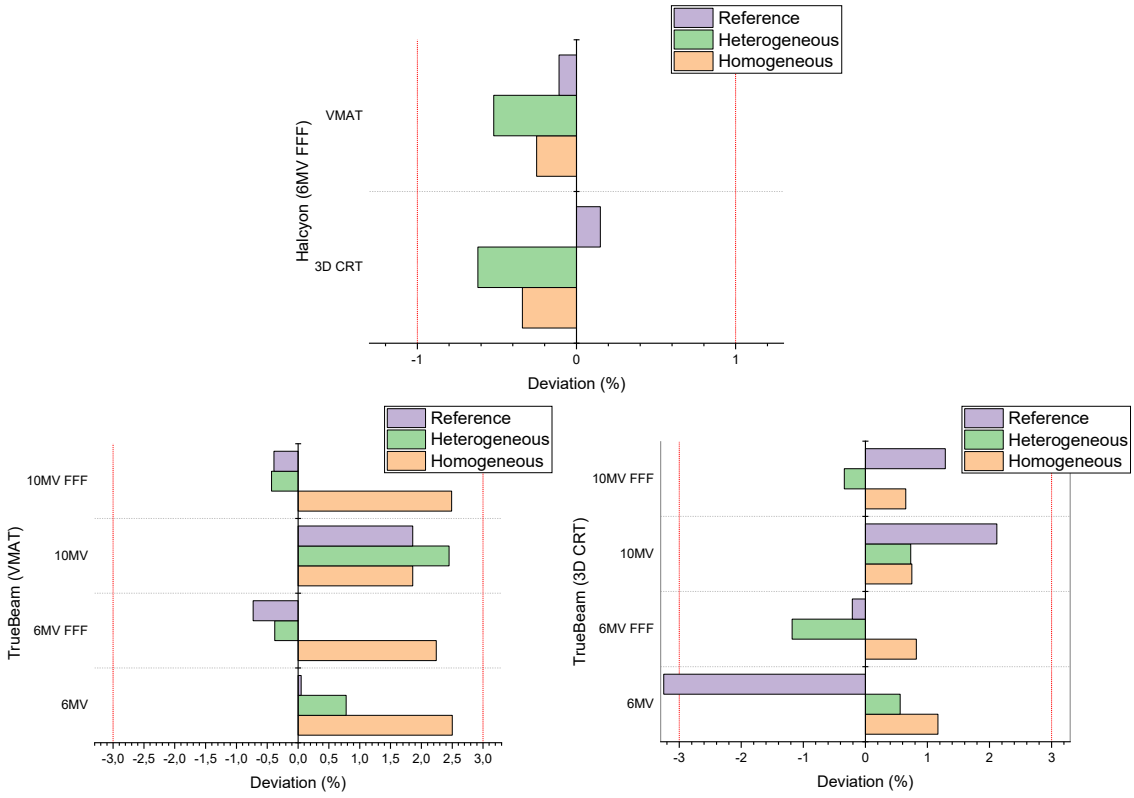

Figure 5. Bar graph of dose deviation by phantom type and beam energy.

3.3 Summary of key findings

The evaluation demonstrated that the 3D-printed homogeneous PMMA phantom provides radiological and dosimetric stability comparable to commercial QA devices. HU values were consistent across kernels with variations within ±5 HU, and dose measurements agreed with TPS calculations within ±2.5% across all energies, delivery techniques, and both accelerators. These results confirm its reliability for clinical end-to-end testing and routine QA.

The heterogeneous phantom showed promising but less stable performance. EVA and gypsum–chalk composites reproduced soft-tissue and bone-like imaging characteristics reliably, whereas PLA and MDI-based foam exhibited excessive HU variability, particularly with high-resolution kernels. Dosimetrically, the heterogeneous phantom-maintained deviations within ±3%, though slightly higher scatter was observed on the TrueBeam compared to the Halcyon.

No systematic differences were identified between 3D-CRT and VMAT deliveries, indicating that phantom performance is robust across both simple and complex treatment techniques. The observed variations are mainly attributable to material selection and, to a lesser extent, accelerator-specific beam modeling and setup factors.

Overall, the findings support the homogeneous phantom as a clinically ready, low-cost QA tool, while the heterogeneous phantom requires further refinement, particularly in material composition, to achieve the same level of stability.

4. DISCUSSION

Our results demonstrate that 3D-printed homogeneous phantoms can achieve HU stability within clinically acceptable ranges and dose agreement with the TPS comparable to commercial standards. This finding aligns with earlier reports that homogeneous 3D-printed materials such as PLA provide reproducible radiological and dosimetric properties suitable for routine QA applications [6, 15, 16].

For heterogeneous phantoms, however, our study confirmed the greater challenges previously described in reproducing tissue-equivalent properties [7, 9, 10]. Variability in HU for bone-equivalent and lung-equivalent regions is consistent with earlier investigations, emphasizing that material selection and printer calibration remain critical factors for accurate tissue simulation. These limitations were also highlighted in end-to-end testing studies, where deviations in HU translated into measurable dose differences in high-gradient regions [8, 10, 11].

At the same time, our approach contributes additional evidence that 3D-printed heterogeneous phantoms are feasible for comprehensive clinical validation. Significantly, our work extends prior evaluations by incorporating end-to-end verification using the VMAT technique, which to date has been rarely investigated in 3D-printed models [10, 12].

Beyond direct phantom performance, our results can also be compared to earlier IMRT commissioning studies [17].

Finally, the broader context of medical physics practice must be considered. The need for accessible, affordable QA solutions is particularly urgent in low- and middle-income countries. Meghzifene et al. highlighted persistent global challenges in medical physics education and training [13], while Zubizarreta et al. documented the critical shortfall in radiotherapy infrastructure in resource-limited settings [18]. Against this background, cost-effective 3D-printed phantoms, as developed in our study, could provide an essential contribution to strengthening QA capacity where it is most urgently needed.

5. CONCLUSIONS

This study demonstrated the feasibility of 3D printing cost-effective phantoms for radiation therapy quality assurance. The homogeneous PMMA phantom demonstrated stable radiological and dosimetric performance comparable to that of commercial devices, whereas the heterogeneous model requires further material refinement to achieve similar reproducibility.

The research was partially supported by the National Research Foundation of Ukraine under the project "Improving Quality and Safety in Radiation Therapy for Cancer and Radiological Diagnostics" with registration number 2021.01/0211 (Science for Safety and Sustainable Development of Ukraine).

ORCID

V. Vashchyshyn, https://orcid.org/0009-0003-0005-1924; **O. Bezshyyko,** https://orcid.org/0000-0001-7106-5213

REFERENCES

[1] IAEA, *Accuracy Requirements and Uncertainties in Radiotherapy.* IAEA Human Health Series No. 31. Vienna: IAEA; 2016.
[2] W. Qiu, H. Sun, Z. Hu, *et al*. "Constructing customized multimodal phantoms through 3D printing. A Preliminary Evaluation," Front Phys. **9**, (2021). https://doi.org/10.3389/fphy.2021.605630
[3] P. Kunert, H. Schlattl, S.S. Trinkl, E. Honorio, D. Reichert, and A.A. Giussani, "3D printing of realistic body phantoms: Comparison of measured and simulated organ doses on the example of a CT scan on a pregnant woman," Med. Phys. **51**(12), 9264-9274 (2024). https://doi.org/10.1002/mp.17420
[4] D. Ma, R. Gao, M. Li, and J. Qiu, "Mechanical and medical imaging properties of 3D-printed materials as tissue-equivalent materials," J. Appl. Clin. Med. Phys. **23**(2), e13495 (2022). https://doi.org/10.1002/acm2.13495
[5] J. Silberstein, and Z. Sun, "Advances and Applications of Three-Dimensional-Printed Patient-Specific Chest Phantoms in Radiology: A Systematic Review," Appl. Sci. **14**(13), 5467 (2024). https://doi.org/10.3390/app14135467
[6] N.E.M. Zain, U. Jais, R. Abdullah, and N.W. Abd Rahman, "Dosimetric characterization of customized PLA phantom for radiotherapy," J. Sains. Nuklear. Malaysia. **31**(2), 1-6 (2019). https://inis.iaea.org/records/7n3ar-vwf37

[7] R. Tino, A. Yeo, M. Leary, M. Brandt, and T. Kron, "A systematic review on 3D-printed imaging and dosimetry phantoms in radiation therapy," Technol. Cancer Res. Treat. (18), (2019). https://doi.org/10.1177/1533033819870208
[8] R.B. Tino, A.U. Yeo, M. Brandt, M. Leary, and T. Kron, "A customizable anthropomorphic phantom for dosimetric verification of 3D-printed lung, tissue, and bone density materials," Med. Phys. **49**(1), 52–69 (2022). https://doi.org/10.1002/mp.15364
[9] N. Kadoya, K. Abe, H. Nemoto, K. Sato, Y. Ieko, K. Ito, S. Dobashi, *et al*. "Evaluation of a 3D-printed heterogeneous anthropomorphic head and neck phantom for patient-specific quality assurance in intensity-modulated radiation therapy," Radiol. Phys. Technol. **12**(3), 351–356 (2019). https://doi.org/10.1007/s12194-019-00527-5
[10] J.W. Yea, J.W. Park, S.K. Kim, D.Y. Kim, J.G. Kim, C.Y. Seo, *et al*. "Feasibility of a 3D-printed anthropomorphic patient-specific head phantom for patient-specific quality assurance of intensity-modulated radiotherapy," PLoS One, **12**(7), e0181560 (2017). https://doi.org/10.1371/journal.pone.0181560
[11] L. Mertens, J. Fleckenstein, V. Steil, and F. Schneider, "A novel end-to-end test for combined dosimetric and geometric treatment verification using a 3D-printed phantom," Med. Dosim. **47**(2), 177–183 (2022). https://doi.org/10.1016/j.meddos.2022.02.002
[12] H. Marshall, T. Selvan, and R. Ahmad, "Evaluation of a novel phantom for the quality assurance of a six-degree-of-freedom couch 3D-printed at multiple centres," Phys. Med. **114**, 103136 (2023). https://doi.org/10.1016/j.ejmp.2023.103136
[13] A. Meghzifene, "Medical physics challenges for the implementation of quality assurance programmes in radiation oncology," Clin. Oncol. (R Coll Radiol), **29**(2), 116–119 (2017). https://doi.org/10.1016/j.clon.2016.10.008
[14] IAEA. Absorbed Dose Determination in External Beam Radiotherapy. Technical Report Series No. 398. Vienna: IAEA; 2000.
[15] Y. Choi, J. Lee, K. Park, R. Park, Y. Cho, J. Kim, and H.H. Lee, "Patient-Specific Quality Assurance Using a 3D-Printed Chest Phantom for Intraoperative Radiotherapy in Breast Cancer," Front Oncol. **11**, 699592 (2021). https://doi.org/10.3389/fonc.2021.699592
[16] A. Chaikh, A. Chaabane, C. Jardin, S. Bassot, T. Beaumont, M. Chea, *et al*. "Modeling and dosimetric characterization of a 3D printed pregnant woman phantom for fetal dosimetry in radiotherapy," Radioprotection. **60**(1), 50–56 (2025). https://doi.org/10.1051/radiopro/2024039
[17] G.A. Ezzell, J.W. Burmeister, N. Dogan, T.J. LoSasso, J.G. Mechalakos, D. Mihailidis, A. Molineu, *et al*. "IMRT commissioning: multiple institution planning and dosimetry comparisons," Med. Phys. **36**(11), 5359–5373 (2009). https://doi.org/10.1118/1.3238104
[18] E.H. Zubizarreta, E. Fidarova, B. Healy, and E. Rosenblatt, "Need for radiotherapy in low and middle income countries – the silent crisis continues," Clin. Oncol. (R Coll Radiol), **27**(2), 107-114 (2015). https://doi.org/10.1016/j.clon.2014.10.006

РОЗРОБКА І ОЦІНКА ГОМОГЕННИХ І ГЕТЕРОГЕННИХ ФАНТОМІВ, НАДРУКОВАНИХ МЕТОДОМ 3D-ДРУКУ, ДЛЯ ЗАБЕЗПЕЧЕННЯ ЯКОСТІ ПРОМЕНЕВОЇ ТЕРАПІЇ

В. Ващишин[1], О. Безшийко[2], Л. Голинка-Безшийко[2]
[1]Відділення променевої терапії, Універсальна клініка «Оберіг», Київ, Україна
[2]Київський національний університет імені Тараса Шевченка, Київ, Україна

Передумови: Доступні та місцеві фантоми контролю якості (QA) мають вирішальне значення для підтримки точності променевої терапії, особливо в умовах обмежених ресурсів. Це дослідження оцінює радіологічні та дозиметричні характеристики 3D-друкованих гомогенних та гетерогенних фантомів порівняно з комерційними стандартами.
Методи: Було розроблено два прототипи фантома: гомогенну модель, виготовлену з PMMA, та гетерогенну модель, що складається з EVA, PLA, піни на основі MDI та гіпсово-крейдяного композиту. Радіологічні властивості оцінювали за допомогою КТ-візуалізації з трьома реконструкційними ядрами (Hp38, Bf39, Hr32) при товщині зрізу 1–3 мм. Одиниці Хаунсфілда (HU) порівнювали з референтними значеннями з Easy Slab (IBA) та CatPhan 604. Дозиметричну валідацію проводили за допомогою Eclipse TPS (v16.1) з використанням 15 3D-CRT та 15 VMAT планів, налаштованих на прискорювачі Varian TrueBeam (6 MV, 6 MV FFF, 10 MV, 10 MV FFF) та Halcyon (6 MV FFF). Точкові дози вимірювали за допомогою каліброваної камери Фармера.
Результати: Гомогенний фантом PMMA продемонстрував стабільність HU в межах ±5 HU від референтних значень для всіх ядер зі стандартними відхиленнями менше 3 HU. EVA та гіпс-крейда забезпечили тканинно-еквівалентні та кістково-еквівалентні властивості візуалізації (20 ± 3 HU та 1200 ± 15 HU відповідно), тоді як PLA та MDI продемонстрували надмірну мінливість (залежність від ядра >40 HU). Дозиметрично, гомогенний фантом досяг узгодженості з розрахунками TPS у межах ±2,5% для всіх енергій та методів. Гетерогенний фантом демонстрував відхилення до 2,8%, залишаючись у межах ±3% допуску AAPM TG-119. Мінливість була найбільш значною для планів VMAT з променями FFF, особливо на платформі Halcyon.
Висновок: Гомогенний фантом з PMMA, надрукований на 3D-принтері, продемонстрував радіологічну стабільність та дозиметричну точність, порівнянну з комерційними пристроями, що підтверджує його доцільність для рутинного контролю якості. Гетерогенна модель продемонструвала прийнятні характеристики, але вимагає вдосконалення матеріалів, зокрема заміни PLA та MDI піни, для покращення стабільності HU. Ці результати підкреслюють потенціал адитивного виробництва для забезпечення економічно ефективних, налаштовуваних рішень контролю якості для променевої терапії, особливо в умовах обмежених ресурсів.
Ключові слова: *забезпечення якості (QA); 3D-друк у медичній фізиці; фантоми візуалізації; комп'ютерна томографія (КТ); стабільність HU; наскрізне тестування; валідація фантома; доступні пристрої для контролю якості*